



## OPEN ACCESS

## EDITED BY

Zhuolun Li,  
Lanzhou University, China

## REVIEWED BY

Jingran Zhang,  
Nanjing Normal University, China  
Jiwei Fan,  
China Earthquake Administration, China

## \*CORRESPONDENCE

Peixian Shu,  
✉ shupx@ieecas.cn

RECEIVED 16 December 2022

ACCEPTED 16 May 2023

PUBLISHED 30 May 2023

## CITATION

Wang C, Qiu Y, Fan F, Li B, Niu D and Shu P  
(2023), Rapid environmental changes in  
the Lake Qinghai basin during the  
late Holocene.  
*Front. Earth Sci.* 11:1125302.  
doi: 10.3389/feart.2023.1125302

## COPYRIGHT

© 2023 Wang, Qiu, Fan, Li, Niu and Shu.  
This is an open-access article distributed  
under the terms of the [Creative  
Commons Attribution License \(CC BY\)](#).  
The use, distribution or reproduction in  
other forums is permitted, provided the  
original author(s) and the copyright  
owner(s) are credited and that the original  
publication in this journal is cited, in  
accordance with accepted academic  
practice. No use, distribution or  
reproduction is permitted which does not  
comply with these terms.

# Rapid environmental changes in the Lake Qinghai basin during the late Holocene

Chen Wang<sup>1</sup>, Yahui Qiu<sup>2,3</sup>, Fenglei Fan<sup>4,5</sup>, Baosheng Li<sup>5</sup>,  
Dongfeng Niu<sup>6</sup> and Peixian Shu<sup>7,8,9\*</sup>

<sup>1</sup>School of Ecology and Environment, Tibet University, Lhasa, Tibet, China, <sup>2</sup>School of Cultural Heritage, Northwest University, Xi'an, China, <sup>3</sup>Ministry of Education Key Laboratory of Cultural Heritage Studies and Conservation, Northwest University, Xi'an, China, <sup>4</sup>Joint Laboratory of Plateau Surface Remote Sensing, Tibet University, Lhasa, Tibet, China, <sup>5</sup>School of Geography, South China Normal University, Guangzhou, China, <sup>6</sup>School of Geography, Lingnan Normal University, Zhanjiang, China, <sup>7</sup>State Key Laboratory of Loess and Quaternary Geology, Institute of Earth Environment, Chinese Academy of Sciences, Xi'an, China, <sup>8</sup>Center for Excellence in Quaternary Science and Global Change, Chinese Academy of Sciences, Xi'an, China, <sup>9</sup>Shaanxi Key Laboratory of Accelerator Mass Spectrometry Technology and Application, Xi'an, China

The Lake Qinghai Basin is sensitive to global and regional climate change because of its unique geographical location. It is the hotspot for paleoclimate research in East Asia. In this study, we reconstructed the environmental evolution of the Lake Qinghai since ~9 ka by using a high-resolution peat and fluvial-lacustrine record (Laoyinggou profile) obtained at the foot of Nanshan Mountain. Based on 8 AMS<sup>14</sup>C dates and lithology, loss on ignition (LOI), total organic matter (TOC), X-ray fluorescence (XRF) core-scanning measurements, ratio of total organic carbon to nitrogen (TOC/TN), and sediment particle sorting coefficients, we show that during the Middle Holocene (~9–4.4 ka BP) this region was primarily dominated by the Asian summer monsoon, with a consistent, warm, and humid environment. By contrast, during the late Holocene (4.4 ka to present), the climatic context in this area fluctuated dramatically at the millennial scales. The low TOC content, lower TOC/TN ration and strong hydroclimatic indicate six rapid climate change events, which occurred at ~4.0 ka, ~3.6 ka, ~3.2 ka, ~2.8 ka, ~2.1 ka, and ~1.4 ka, all of which coincided to cold episodes in the North Atlantic Ocean.

## KEYWORDS

Lake Qinghai basin, high-resolution record, rapid climate change (RCC), late Holocene, cold events

## 1 Introduction

The Holocene climate was generally warm and stable at the orbital scale, but numerous studies have demonstrated that the instability of the climate during the Holocene was associated with a number of rapid climate change (RCC) events at the millennial-centennial scales (Bond et al., 1997; Bond et al., 2001; Wang et al., 2005). These RCC events are mainly characterized by cooling in the mid-high latitudes of the Northern Hemisphere and drought in the low-latitude monsoon regions. Paleoclimate communities have comprehensively studied the 8.2 thousand years (ka) event (Alley et al., 1997; Alley and Agustsdottir, 2005) and 4.2 ka event (Weiss, 2019; Utida et al., 2020; An et al., 2021), recognized 2 climate anomalies globally. These 2 RCC events as time nodes could be divided into Early Holocene

(11.5–8.2 ka), Middle Holocene (8.2–4.2 ka) and Late Holocene (4.2 ka to present) (Zanchetta et al., 2016; Ran and Chen, 2019; Walker et al., 2019).

Lake Qinghai, the largest inland lake in China, is located on the northeastern margin of the Qinghai-Tibet Plateau (An et al., 2012). It is located at the front of the Asian summer monsoon and has a high altitude, which makes it very sensitive to the climate change of the East Asian monsoon, Indian monsoon and westerly belt, and has become the hot spot for studying the interaction of these paleoclimate systems (Lister et al., 1991; Shen et al., 2005; An et al., 2012; Liu et al., 2014; Thomas et al., 2014). In the past few decades, many scholars have done a lot of studies on the paleoclimate and environmental evolution of the sediments in the Lake Qinghai Basin. An et al. (2012) revealed that the cold-dry events around 11.0 ka, 10.3 ka, 9.3 ka, 7.2 ka and 5.5 ka, and suggested that the millennial-scale climate change in the Lake Qinghai during the Holocene reflects that Summer Monsoon Index (SMI) variability may be linked to North Atlantic abrupt events associated with the Atlantic's overturning circulation and sea-ice variations, freshwater forcing played a prominent role in millennial scale climate change. Furthermore, weak monsoon events in the SMI sequence can be correlated with many of the intervals of low solar activity (An et al., 2012). Ji et al. (2005) argued that the 8.2 ka event and the Little Ice Age event were recorded in the Lake Qinghai sediments. Wang et al. (2015) reconstructed the palaeotemperature of the Lake Qinghai using long chain alkenones, exhibits 10.4 ka and 8.8 ka rapid climate changes. Besides lake sediments, aeolian sand and loess surrounding Lake Qinghai areas also record the rapid climate change during the Holocene (Lu et al., 2010; Liu et al., 2012; Shang et al., 2013; E et al., 2015; Lu et al., 2015; Ding et al., 2019; E et al., 2019; Yang et al., 2019). For example, the eastern sandy land of the Lake Qinghai has obvious response to 9.4 ka, 8.2 ka and 4 ka cold events (Liu, 2013; Lv, 2018).

Recently, Yang et al. (2021) analyzed the stable isotope record of the Delingha tree rings on the western side of the Lake Qinghai, providing high-resolution Holocene paleoclimate data for the region (Yang et al., 2021). According to Yang et al. (2022) the record does not reflect a significant hydroclimatic transition event occurring around 4.2 ka (Yang et al., 2022). However, Weiss (2022) argued that Delingha tree rings recorded the 4.2 ka event. Therefore, how many Holocene abrupt climate events existed in the Lake Qinghai Basin, especially whether there was a 4.2 ka event, still need more paleoclimatic records to discuss.

Peat has a high content of organic matter, and radiocarbon ( $^{14}\text{C}$ ) dating of peat, which is not easy to be affected by the hard water effect, and can provide independent age-paleoclimatic information different from saltwater lake deposition and eolian deposition records (Geyh et al., 1997; Hatté et al., 2001; Wang et al., 2014; Zhou et al., 2022). As a result, peat is convenient and accurate for  $^{14}\text{C}$  dating in paleoclimatology research. In addition, peat deposition has good continuity and high resolution, and a variety of indicators can interpret rich environmental information. Thus, the change of peat deposition comprehensively reflects the change of sedimentary environment and hydrological conditions. To date, However, there exists a limited number of studies linked to the rapid change in climate and hydrological

conditions within the Holocene of the Lake Qinghai Basin, utilizing peat as a means of paleoclimatology study. Given this, we selected to utilize the Laoyinggou (LYG) peat deposition profile situated at the northern base of Nanshan Mountain in the southwestern region of Lake Qinghai to reconstruct climate variations dating back to 9 ka BP.

## 2 Study area

The Lake Qinghai Basin is located in the northeastern part of the Qinghai-Tibet Plateau (Figure 1), with an altitude of 3,100–4,755 m, surrounded by the Datong Mountains in the north, the Riyue Mountains in the east and the Nanshan Mountains in the southwest, covering a total area of 29,000 square kilometers. The climate is plateau continental climate, winter is cold and long, summer is cool and short, and spring is windy with sandstorms, less rainfall, wet and dry seasons are clear. The basin has a variety of habitats, including alpine shrub, cold temperate coniferous forest, temperate grassland, alpine meadow, marsh meadow and sandy vegetation, etc. (Chen, 1993; Chen et al., 2011).

## 3 Materials and methods

LYG profile (Figure 1; Figure 2) is located on the east bank of a tributary extending southward from Jiangxi Gully on the southern bank of the Lake Qinghai. This profile is a peat and fluvial-lacustrine deposit cut by a modern river, the coordinates are 36°32'05.07"N, 100°18'15.95"E, the altitude is 3438 m, and the linear distance from the modern Lake Qinghai shoreline is 13–15 km. The profile is 300 cm thick and can be divided into the two parts according to lithology.

0–135 cm, visible obvious plant roots at the top, black to brown sandy clayey silt, peat layer containing more humus plants, which can be divided into the following layers.

0–30 cm: brownish meadow soil with clayey sandy silt, with more grass roots and occasional shrub roots.

31–40 cm: brownish-black clayey sandy silt.

41–55 cm: black peat layer, with many humus plants.

56–90 cm: brownish-gray sandy clayey silt, with thin layers of peat at 65 cm, 82 cm.

91–105 cm: black peat layer, mostly humus.

106–115 cm: brownish gray sandy clayey silt, weakly developed soil aggregates, brownish patches visible.

116–125 cm: light grey clayey sandy silt.

126–135 cm: black peat layer with mostly humus plants.

136–300 cm: black-brown to grayish-yellow, gravelly clayey sandy silt, which can be divided into the following layers.

136–155 cm: black-brown gravelly sandy clayey silt with weakly developed soil.

156–175 cm: grayish-yellow clayey sandy silt, sand with fine gravels, interspersed with black organic matter layer, oxidized plant roots visible, weakly developed soil-on lacustrine sediments.

176–285 cm: brownish-black gravelly sandy clayey silt with gravels.

286–300 cm: grayish-white clayey sandy silt.

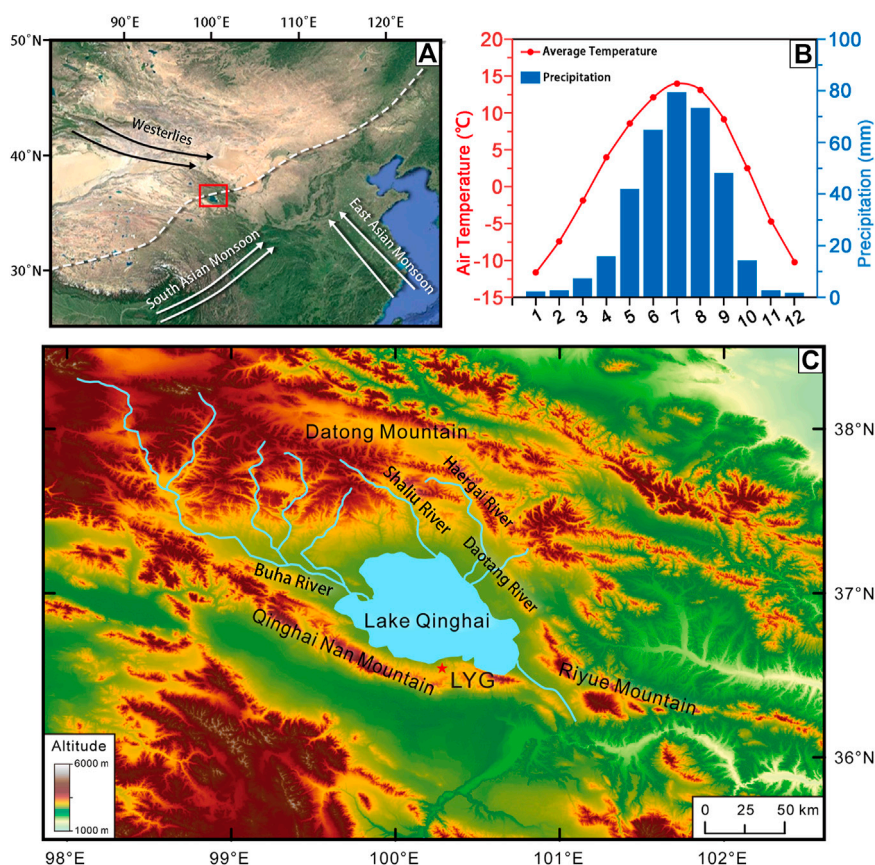


FIGURE 1

Physiographical map of the study site (red solid star, LYG profile,  $36^{\circ}32'05.07''N$ ,  $100^{\circ}18'15.95''E$ , 3438 m). (A) Overview map showing locations of the Lake Qinghai Basin, and the dominant circulation systems of the westerlies and the Asian monsoon.; (B) Monthly mean precipitation and temperature changes from 1959 to 2015 (Ding et al., 2018); (C) Location of Lake Qinghai and the LYG profile site.

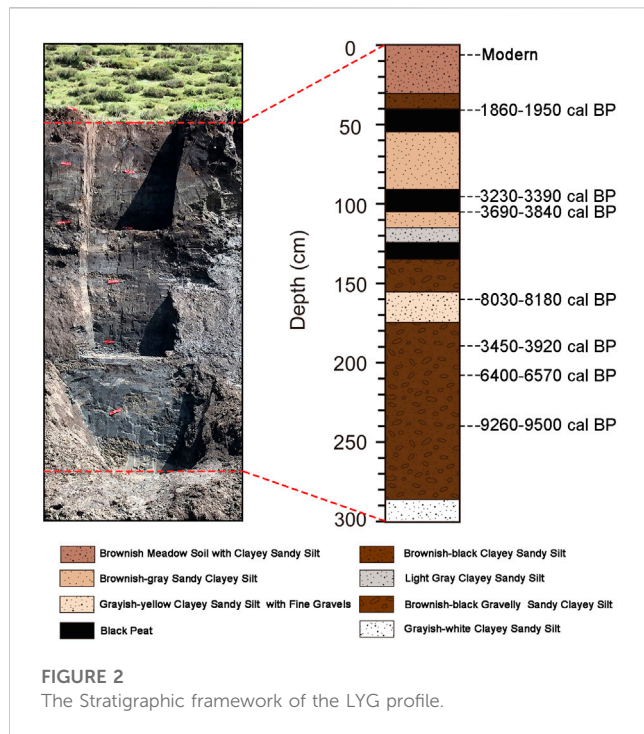
Before sampling, we cleaned the surface layer of the profile, and removed 5–10 cm of soil on its surface to expose the fresh profile, and then used the columnar stainless-steel groove to sample, so that the complete and continuous samples were taken, which was convenient for the X-ray fluorescence (XRF) scanning analysis. The core samples were divided at 1 cm intervals in the laboratory. Samples 101 and 102 (at the depths of 101 and 102 cm) are missing due to compression.

### 3.1 Chronology

We selected organic matter samples from 6 horizons, plant residues and freshwater snail shells from 3 horizons in the LYG profile to conduct Accelerator Mass Spectrometry (AMS)  $^{14}C$  dating. The results are shown in Table 1. The results of AMS  $^{14}C$  dates were calibrated with IntCal 20 dataset in Calib 8.1 program with 2 sigma uncertainty. The AMS  $^{14}C$  dating of the LYG sediment profile was conducted by the BETA Laboratory and Xi'an-AMS Center.

### 3.2 Sediment analysis

Loss on ignition (LOI) measurements were determined at 1 cm intervals using KSL-1000X-M, weighed the appropriate amount of samples in the crucible, set  $550^{\circ}C$  burning 3 h (Heiri et al., 2001; Santisteban et al., 2004). Elemental measurements were determined at 1 cm intervals using an Avaatech XRF scanner (Richter et al., 2006; Liang et al., 2012; Davies et al., 2015; Sun et al., 2016; Guo et al., 2021). TOC concentrations were measured at 4 cm intervals with a Costech ECS4010/4024 cube analyzer, with a measurement uncertainty of  $<0.1\%$ . Total Nitrogen (TN) content was also measured simultaneously in order to calculate TOC/TN. Grain size analysis was made at 2 cm intervals with a Malvern Mastersizer 3000 laser-diffraction analyzer, which determines grain sizes of  $0.01\text{--}3000\ \mu m$ , with an analytical error within 2% (Sun et al., 2006; An et al., 2012). The grain size data were analyzed using the open source software QGrain (Liu et al., 2021). The above experiments were done at the Institute of Earth Environment, Chinese Academy of Sciences. All results are shown in Figure 4.



## 4 Results

### 4.1 Age model

Nine <sup>14</sup>C dating results (Table 1) are generally consistent with the stratigraphic sequence, except for LYG160. We selected two different organic materials (TOC and plant residues) for AMS <sup>14</sup>C dating at 190 cm depth in the LYG profile, and the results showed that the <sup>14</sup>C age of LYG190 organic matter and plant residues were 3290 ± 30 a BP and 3520 ± 45 a BP, respectively. After calibration, organic matter and plant residues reflected a

consistent range of ages. Therefore, we used 8 <sup>14</sup>C ages except LYG160, and the Bacon model (Blaauw and Christen, 2011) in R software was used for age and depth interpolation and extrapolation to obtain the age results of 0–300 cm for this profile. The deposition rate of 0–300 cm in this profile is calculated in the model, and the results are shown in Figure 3.

### 4.2 Chemical and physical characteristics of the LYG sediments

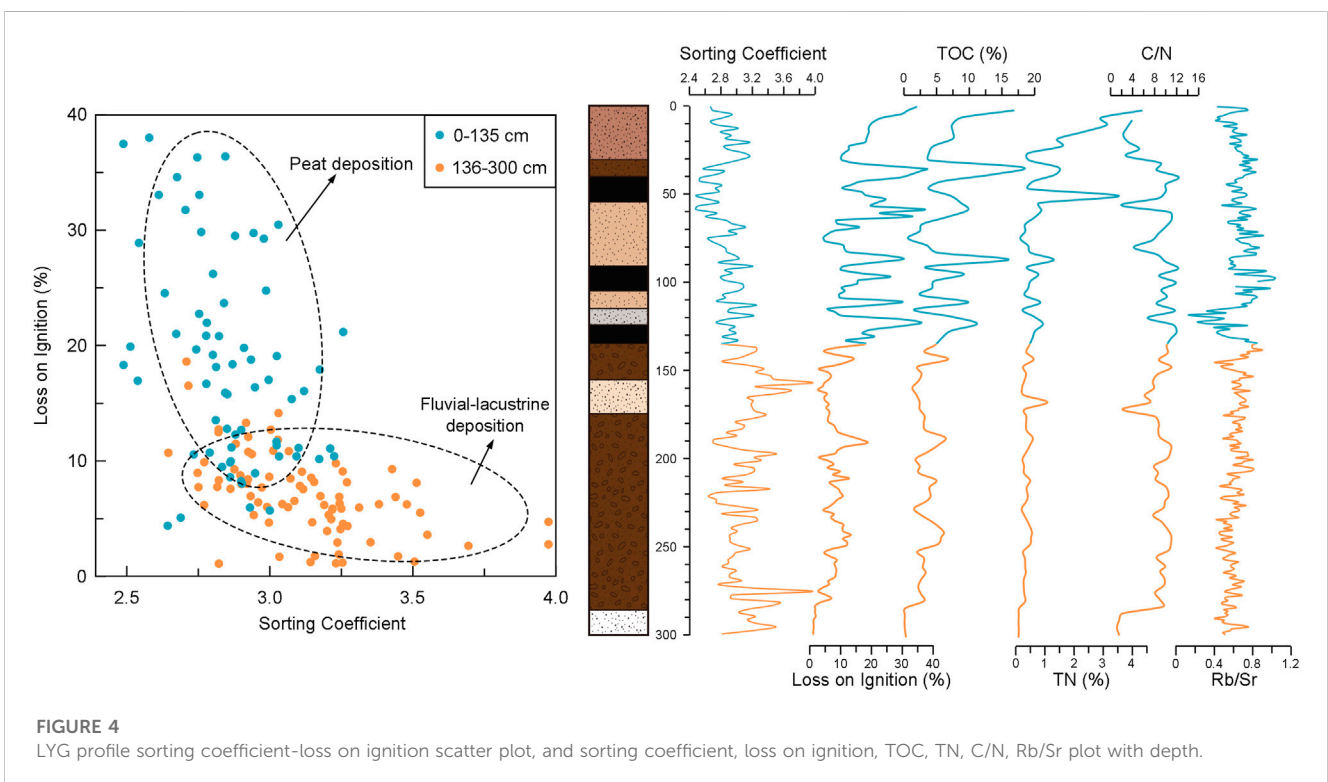
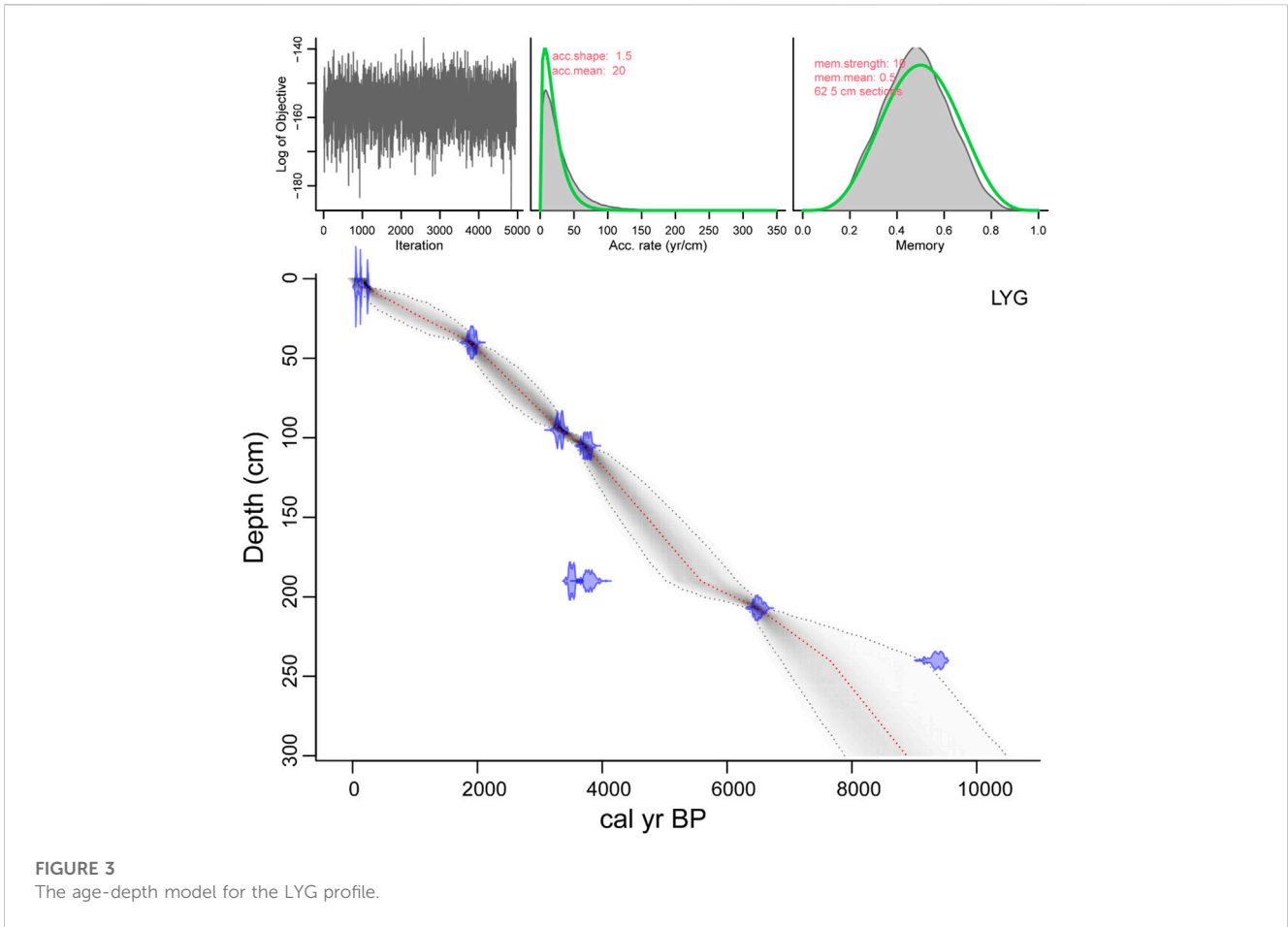
The sediment particle sorting coefficient varies from 2.49 to 3.97 (Figure 4), with an average value of 3.00. The LOI varies from 0.83% to 39.26% (Figure 4), with an average value of 12.34%. The TOC/TN varies from 1.22 to 12.42 (Figure 4), with an average value of 8.32. The Rb/Sr ratio varies from 0.14 to 1.04 (Figure 4), with an average value of 0.63.

Based on particle sorting coefficient, LOI, XRF results, TOC/TN and Rb/Sr ratio results, combined with the sedimentological observations in the field, the LYG profile can be roughly divided into two units from bottom to top, with the boundary at 135 cm (Figure 4):

- 1) 136–300 cm, which is the fluvial-lacustrine unit. This sediments unit has high particle size sorting coefficient values, with average value of 3.12. The LOI indicates low organic matter content (average value of 7.25) and good agreement with TOC content. TOC/TN ratio is low than 10. The Rb/Sr ratio is also low, with average value is 0.61.
- 2) 1–135 cm, a peat sedimentary unit. The sediments are mostly clay, and the particle size sorting coefficient is much lower than that of the fluvial-lacustrine unit, with average value is 2.88. The LOI is significantly higher than the previous unit (average value is 18.49). Average value of TOC/TN ration is 8.40. Rb/Sr rises to the highest value (~1.04), which also indicates that the intensity of regional weathering in the basin decreases compared to the previous interval.

TABLE 1 AMS<sup>14</sup>C dates of LYG profile.

Sample number	Depth (cm)	Laboratory number	Dating material	<sup>14</sup> C age (a B.P.)	Calibration age
					(Cal.a B.P., 2σ error)
LYG005	5	Beta532345	Organic matter	Post-Bomb data	—
LYG040	40	Beta532346	peat	1980 ± 30	1860–1950
LYG095	95	Beta532347	peat	3110 ± 30	3230–3390
LYG105	105	Beta532348	Organic matter	3480 ± 30	3690–3840
LYG160	160	Beta532349	Organic matter	7330 ± 30	8030–8180
LYG190	190	Beta532350	Organic matter	3290 ± 30	3450–3570
LYG190	190	XA23475	Plant residue	3520 ± 45	3690–3920
LYG207	207	XA23476	Plant residue	5710 ± 40	6400–6570
LYG240	240	XA23548	Snail shell	8360 ± 60	9260–9500



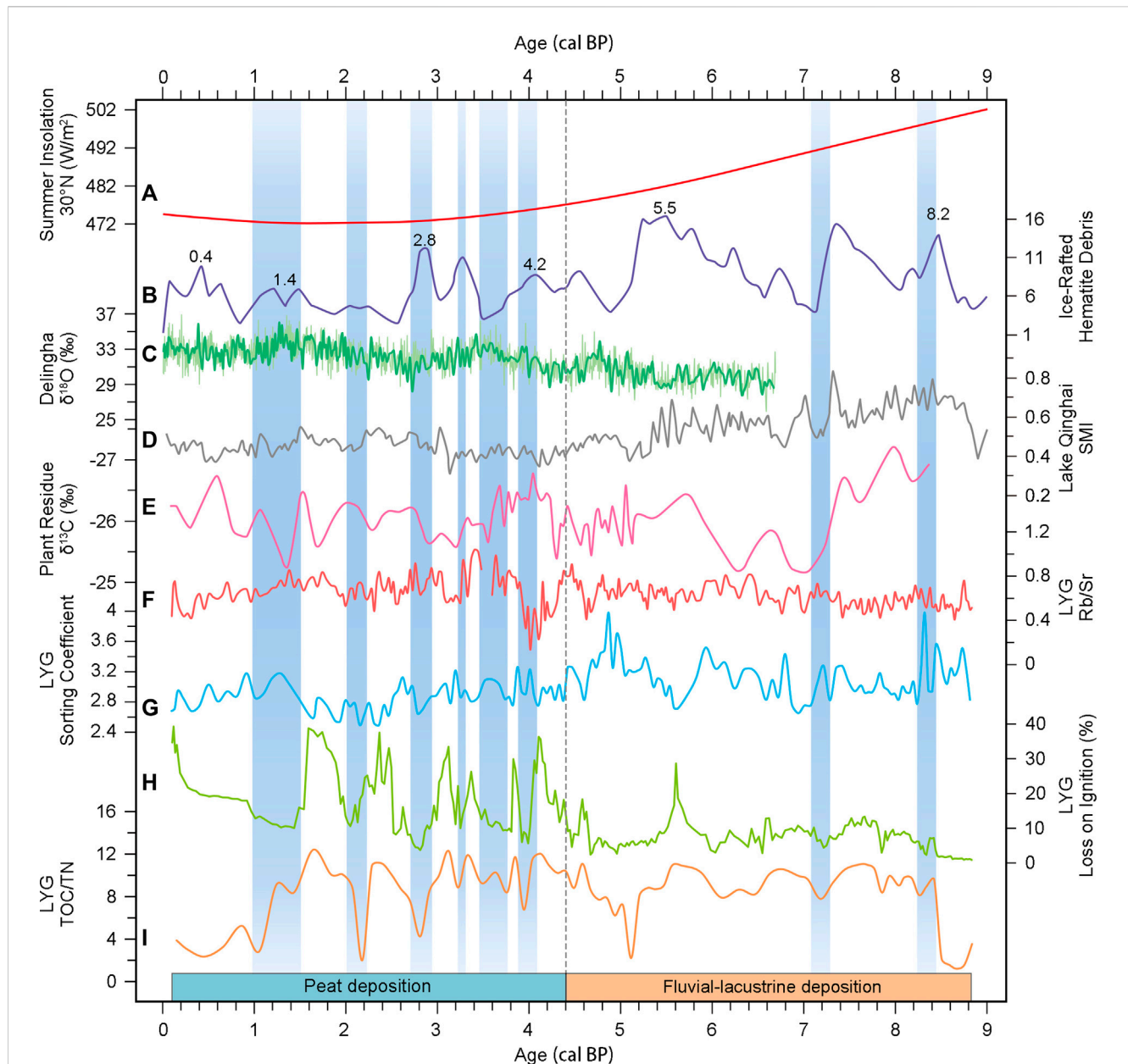


FIGURE 5

Comparison of Mid-to Late Holocene Environmental Records and Regional Climate of LYG profile. (A) 30°N Summer Insolation (Laskar et al., 2011); (B) Ice-Rafted Hematite Debris (IRD) (Bond et al., 2001); (C)  $\delta^{18}\text{O}$  from Delingha tree rings (An et al., 2021); (D) Asian summer monsoon index inferred from Lake Qinghai (An et al., 2012); (E)  $\delta^{13}\text{C}$  values of terrestrial plant fragments from the HYSX profile in the Lake Qinghai region (Li et al., 2018); (F) Rb/Sr of LYG profile; (G) sorting coefficient of LYG profile; (H) LOI of LYG profile; (I) TOC/TN of LYG profile.

## 5 Discussion

### 5.1 Characteristics of the Holocene environment changes

Some studies have shown that the determination of organic matter in stratigraphic profiles can provide a basis for recovery of past environmental changes to a certain extent (Zhang, 1998). The productivity of organic matter in arid regions is regulated by the impact of precipitation, as noted by An et al. (1993). Chen et al. (2003) have observed that enhanced precipitation not only enhances

productivity in lake, but also serves as a crucial factor in the preservation of organic material within the lake. In general, during the humid period, the water level of the lake rose, which became a lacks oxygen environment and conducive to the preservation of organic matter. On the contrary, the content of organic matter in the sediment decreases (Liu, 2012). Moreover, TOC/TN can be used to distinguish endogenous and exogenous organic matter in lake sediments (Meyers, 1990; Talbot and Johannessen, 1992; Meyers, 1994; Lamb et al., 2006). Aquatic phytoplankton are relatively rich in proteins, which are rich in organic nitrogen, so the endogenous C/N from organic matter is

low, usually between 4 and 10. Terrestrial vascular plants are mainly lignin and cellulose, which have very low nitrogen content, thus the C/N ratio of exogenous organic matter is often greater than 20 and even as high as 100 (Meyers, 1990). Although the LYG profile has a sedimentary phase change, and the sorting coefficient can better reflect the hydrodynamic changes in the profile. The research shows that the standard deviation of sediment reflects the degree of sorting, the higher value represents the lower the degree of sorting, the stronger the hydrodynamic force (Chen and Wan, 1999). Rb appears inert during weathering and remains in the residue fraction in parent rocks as residual silicate, often accumulating in clay minerals (Koinig et al., 2003). In general, Rb and silicates are carried to basin areas (lakes) by physical weathering. Sr is one of the alkaline Earth metal elements, which can form soluble bicarbonate, chloride and sulfate into aqueous solution. Sr is often attached to the surface of carbonate or organic matter in sediments, and is eventually transferred to lake deposits as ions ( $\text{Sr}^{2+}$ ). Therefore, the chemical weathering intensity of the basin is strong, and the Sr content in the corresponding lake sediments will also increase. Therefore, the Rb/Sr ratio can be used as a proxy to indicate the summer monsoon intensity (Gallet et al., 1996; Chen et al., 2001). It has also been found that low Rb/Sr ratios reflect stronger transport of terrigenous detrital material under weak chemical weathering in the basin (Kalugin et al., 2005).

Here, we use the LOI of the organic matter to represent effective humidity, grainsize sorting coefficient to represent regional hydrodynamics, TOC/TN ratio to represent vegetation changes, and Rb/Sr ratio to represent weathering intensity in peats and fluvial-lacustrine records to reconstruct the climate and environment changes since 9 ka in the LYG area. (Figure 5). We divided the study interval into two substages for discussion.

The first stage in 9–4.4 ka BP is a wet period. During this period, the strong summer solar radiation (Figure 5A), strengthening the summer monsoon (Figure 5D) with sufficient precipitation. Average value of TOC/TN ratio in LYG is 8.40, which indicates that the organic matter originated from aquatic plants. At this time, the physical properties of sedimentary profiles with high grainsize sorting coefficients reflect a stronger hydrodynamic. All of these proxies confirm the fluvial-lacustrine deposition environment (Figure 5G). Ma et al. (2011) integrated the multiple records on the fluctuation of the surface of the Lake Qinghai and the  $\delta^{18}\text{O}$  records of the ostracod shells of QH-2000 pore in the Lake Qinghai to show that the surface of the Lake Qinghai was relatively stable at an altitude of 3213 m from 9 to 6 ka, which was ~20 m higher than the modern surface of the lake water. Liu (2018) reanalyzed the palaeoenvironmental records and climate model simulations of in the Lake Qinghai and found that the Holocene climatic optimum period occurred from 8 to 6 ka. The vegetation in the basin was dominated by forests and grasslands, and the water level of the lake was rising during the middle Holocene (Liu, 2018). Aeolian records located around the Lake Qinghai, for example, Zeku profile (Hu et al., 2022), eastern sandy land profile (Lu et al., 2015; Ding et al., 2019; Chen, 2021), Jiangxigou Profile (E et al., 2013; Yang et al., 2016), Xiala Reservoir in Qinghai Nanshan, and Xiangpi Mountain Loess Profile (Chang, 2016) all indicated that the aeolian activity was weak, and most dunes were stabilized.

From 4.4 ka and continuing to the present day, the second stage has been characterized as a period of low temperatures and reduced precipitation. The decreased summer solar radiation

(Figure 5A) during this period weakened the summer monsoon, and the increased Rb/Sr ratio (Figure 5F) also indicates poor regional hydrothermal conditions. The sedimentation profiles and reduced sorting coefficients (Figure 5G) indicate that the shrinkage of watersheds until final disappearance, and LYG profiles shift from fluvial-lacustrine deposition to peat deposition. TOC/TN (Figure 5I) indicates that plant organic matter still originated from aquatic plants. In addition, the weak reducing environment of peat and colder climatic conditions favor the preservation of organic matter, thus the loss on ignition shows high values (Figure 5H). The aeolian sedimentary profile around the Lake Qinghai shows that the aeolian sand activity intensified, the climate deteriorated at ~4.5 ka, and the whole was mainly cold and dry, with a low degree of chemical weathering (E et al., 2013; Lu et al., 2015; Chang, 2016; Yang et al., 2016; Lv, 2018; Ding et al., 2019; Chen, 2021; Hu et al., 2022).

## 5.2 Rapid hydroclimatic change in the Lake Qinghai basin during the Late Holocene

Although the 8.2 ka cold event was the strongest cold event since 11.5 ka in the Holocene, here the LYG region did not respond strongly to it, and the organic matter only showed a weak trough (drops ~5%). This is probably because the organic matter content is not high in the first place, and thus the variation is moderate. However, the LYG profile shows strong fluctuations in organic matter during the Late Holocene, with six rapid hydrological changes (blue stripes in Figure 5) recorded at ~4.0 ka, ~3.6 ka, ~3.2 ka, ~2.8 ka, ~2.1 ka and ~1.4 ka, respectively. These six declines in organic matter (from ~30% to ~10%) are highly consistent with the peak of the North Atlantic ice rafted debris (IRD) events (Figure 5B). Therefore, we focus on these six rapid hydroclimatic changes in the Late Holocene.

Bond et al. (1997) identified nine IRD events in the North Atlantic during the Holocene based on IRD, which were later gradually referred to as cold events. Among them, the cold events that occurred in the late Holocene were 0.4 ka, 1.4 ka, 2.8 ka and 4.2 ka (Figure 5B), and the corresponding numbers were 0–4 (Bond et al., 1997; Bond et al., 2001). In this study, except for 0.4 ka, the LYG profile responds to the other 3 cold events.

Among those cold events, the LYG profile has the strongest response to the 4.2 ka North Atlantic IRD event at ~4.0 ka. The organic matter (Figure 5H) decreased ~30%. The summer monsoon in the Lake Qinghai Basin (Figure 5D) weakened, with a corresponding decrease in precipitation. Secondly, the duration of the rapid hydroclimatic change of ~2.8 ka is longer. The organic matter (Figure 5H) decreases and remains at a low value (the minimum is ~3.6%). The  $\delta^{18}\text{O}$  value of the Delingha tree ring (Figure 5C) was in the low value zone, with a minimum value of ~28‰. In addition, the rapid hydroclimatic change in ~1.4 ka period lasted much longer (~500 years) and had the strongest impact. During this period, the low value of organic matter (Figure 5H) indicated vegetation coverage decreased, and it did not recover until nearly 100 years ago. Affected by the cold event, terrestrial  $\text{C}_3$  vegetation in the Lake Qinghai Basin decreased significantly (Figure 5E). The  $\delta^{18}\text{O}$  of Delingha tree ring also shows a continuous decreasing trend (Figure 5C). Although not labelled

as specific cold events, both ~3.2 ka and ~2.1 ka coincides with the peak of the North Atlantic IRD event (Figure 5B). The Lake Qinghai Basin summer monsoon (Figure 5D) weakened to different degrees in these two periods. Unlike all the above five cold events, there was also a rapid and prolonged hydroclimatic change at 3.6 ka, but this event is not associated with the North Atlantic IRD event (Figure 5B), which may be a regional feature of this region or dating uncertainty.

## 6 Conclusion

We selected the LYG profile, a peat and lacustrine profile at the northern foot of the Nanshan Mountains, to analyze its organic matter, Rb/Sr ratio changes. We combined the results of AMS <sup>14</sup>C dating results to reconstruct the depositional environment of the Lake Qinghai Basin since 9 ka. Based on the experimental results and sedimentary characteristics, we divided the LYG profile into two substages:

- 1) 9–4.4 ka BP, warm and wet period. This stage is characterized as fluvial-lacustrine deposition and the organic matter content in the sediment is not high.
- 2) 4.4 ka BP to date, cold and dry period. The LYG profile changes from fluvial-lacustrine deposition to peat deposition, preserving a large amount of organic matter. In addition, the organic matter records 6 obvious rapid hydroclimatic changes, which occurred at ~4.0 ka, ~3.6 ka, ~3.2 ka, ~2.8 ka, ~2.1 ka, ~1.4 ka. These rapid hydrologic changes were highly consistent with the peak of the North Atlantic IRD event.

## Data availability statement

The original contributions presented in the study are included in the article/supplementary material, further inquiries can be directed to the corresponding author.

## Author contributions

CW formal analysis, investigation, data curation, writing original draft, visualization. YQ methodology, resources, data

curation, review and editing. FF validation, review and editing. BL and PS conceptualization, validation, review and editing, supervision. DN validation and review. PS conceptualization, writing—review and editing, supervision. All authors contributed to the article and approved the submitted version.

## Funding

This study was supported by the Fund of Shandong Province (No. LSKJ202203300), the National Natural Science Foundation of China (Nos. 42030512, 42102237), the Strategic Priority Research Program of the Chinese Academy of Sciences (CAS) (Grant No. XDB 40000000). PS also acknowledges the support of the special research assistant project of the Chinese Academy of Sciences.

## Acknowledgments

We thank Guoqing Zhao and Shugang Wu of the Xi'an Accelerator Center, Institute of Earth Environment, Chinese Academy of Sciences, for their guidance and assistance in the experiments. We thank Prof. Hong Wang of Beijing Normal University for the improvements in English.

## Conflict of interest

The authors declare that the research was conducted in the absence of any commercial or financial relationships that could be construed as a potential conflict of interest.

## Publisher's note

All claims expressed in this article are solely those of the authors and do not necessarily represent those of their affiliated organizations, or those of the publisher, the editors and the reviewers. Any product that may be evaluated in this article, or claim that may be made by its manufacturer, is not guaranteed or endorsed by the publisher.

## References

- Alley, R. B., and Agustsdottir, A. M. (2005). The 8k event: Cause and consequences of a major Holocene abrupt climate change. *Quat. Sci. Rev.* 24, 1123–1149. doi:10.1016/j.quascirev.2004.12.004
- Alley, R. B., Mayewski, P. A., Sowers, T., Stuiver, M., Taylor, K. C., and Clark, P. U. (1997). Holocene climatic instability: A prominent, widespread event 8200 yr ago. *Geology* 25, 483–486. doi:10.1130/0091-7613(1997)025<0483:hciapw>2.3.co;2
- An, Z., Porter, S. C., Zhou, W., Lu, Y., Donahue, D. J., Head, M., et al. (1993). Episode of strengthened summer monsoon climate of Younger Dryas age on the Loess Plateau of central China. *Quat. Res.* 39, 45–54. doi:10.1006/qres.1993.1005
- An, Z., Colman, S. M., Zhou, W., Li, X., Brown, E. T., Jull, A., et al. (2012). Interplay between the westerlies and asian monsoon recorded in lake Qinghai sediments since 32 ka. *Sci. Rep.* 2, 619. doi:10.1038/srep00619
- An, J., Kirleis, W., and Jin, G. (2021). Understanding the collapse of the longshan culture (4400–3800 BP) and the 4.2 ka event in the haidai region of China—from an agricultural perspective. *Environ. Archaeol.*, 1–15. doi:10.1080/14614103.2021.2003583
- Blaauw, M., and Christen, J. A. (2011). Flexible paleoclimate age-depth models using an autoregressive gamma process. *Bayesian anal.* 6, 457–474. doi:10.1214/11-ba618
- Bond, G., Showers, W., Cheseby, M., Lotti, R., Almasi, P., Demenocal, P., et al. (1997). A pervasive millennial-scale cycle in North Atlantic Holocene and glacial climates. *Science* 278, 1257–1266. doi:10.1126/science.278.5341.1257
- Bond, G., Kromer, B., Beer, J., Muscheler, R., Evans, M. N., Showers, W., et al. (2001). Persistent solar influence on North Atlantic climate during the Holocene. *Science* 294, 2130–2136. doi:10.1126/science.1065680
- Chang, Q. (2016). “Study on photoluminescence chronology of aeolian deposits in Nanshan, Qinghai,” in *Journal of salt lake research*. Editors Z. L. Baoliang Lu, F. Han, and X. Xie.
- Chen, J. A., and Wan, G. (1999). Sediment particle size distribution and its environmental significance in Lake Erhai, Yunnan Province. *Chin. J. Geochem.* 18, 314–320. doi:10.1007/bf03052905

- Chen, J., Wang, Y., Chen, Y., Liu, L., Ji, J., and Lu, H. (2001). Rb and Sr geochemistry characteristics of Chinese loess strata and their monsoon significance. *Acta Geol. Sin.* 75, 8.
- Chen, C.-T. A., Lan, H.-C., Lou, J.-Y., and Chen, Y.-C. (2003). The dry Holocene megathermal in inner Mongolia. *Palaeogeogr. Palaeoclimatol. Palaeoecol.* 193, 181–200. doi:10.1016/s0031-0182(03)00225-6
- Chen, K., Han, Y., Cao, S., Ma, J., Cao, G., and Lu, H. (2011). The study of vegetation carbon storage in Qinghai Lake Valley based on remote sensing and CASA model. *Procedia Environ. Sci.* 10, 1568–1574. doi:10.1016/j.proenv.2011.09.249
- Chen, G. (1993). "Vegetation and its distribution of Lake Qinghai area," in *Chinese journal of plant ecology*. Editor M. Peng.
- Chen, D. (2021). "Environmental changes since the middle and late Holocene recorded by He-Lake-Eolian sediments in the sandy land of hudong, qinghai lake," in *Journal of desert research*. Editors Z. D. Lurui Jie and X. Liu.
- Davies, S. J., Lamb, H. F., and Roberts, S. J. (2015). "Micro-XRF core scanning in palaeolimnology: Recent developments," in *Micro-XRF studies of sediment cores*, 189–226.
- Ding, Z., Lu, R., Liu, C., and Chen, D. (2018). "Characteristics of climate change and its monsoon circulation factors in the Qinghai Lake Rim," in *Advances in earth science*.
- Ding, Z., Lu, R., Lyu, Z., and Liu, X. (2019). Geochemical characteristics of Holocene aeolian deposits east of Qinghai Lake, China, and their paleoclimatic implications. *Sci. Total Environ.* 692, 917–929. doi:10.1016/j.scitotenv.2019.07.099
- E, C., Cao, G., Hou, G., Sun, Y., Jiang, Y., and Li, F. (2013). Environmental evolution of loess record in Jiangxi gully, qinghai lake, China. *Mar. Geol. Quat. Geol.* 33, 193–200. doi:10.3724/sp.j.1140.2013.040193
- E, C., Lai, Z., Hou, G., Cao, G., Sun, Y., Wang, Y., et al. (2015). Age determination for a Neolithic site in northeastern Qinghai-Tibetan Plateau using a combined luminescence and radiocarbon dating. *Quat. Geochronol.* 30, 411–415. doi:10.1016/j.quageo.2015.01.007
- E, C., Zhang, J., Chen, Z., Sun, Y., Zhao, Y., Li, P., et al. (2019). High resolution OSL dating of aeolian activity at qinghai lake, northeast Tibetan plateau. *Catena* 183, 104180. doi:10.1016/j.catena.2019.104180
- Gallet, S., Jahn, B. M., and Torii, M. (1996). Geochemical, mineralogical characterization of the Luochuan loess-paleosol sequence, China, and paleoclimatic implications. *Chem. Geol.* 133, 0–88. doi:10.1016/S0009-2541(96)00070-8
- Geyh, M. A., Schotterer, U., and Grosjean, M. (1997). Temporal changes of the  $^{14}\text{C}$  reservoir effect in lakes. *Radiocarbon* 40, 921–931. doi:10.1017/s003822200018890
- Guo, F., Clemens, S., Liu, X., Long, Y., Li, D., Tan, L., et al. (2021). Application of XRF scanning to different geological archives. *Earth Space Sci.* 8, e2020EA001589. doi:10.1029/2020ea001589
- Hatté, C., Pessenda, L. C., Lang, A., and Paterne, M. (2001). Development of accurate and reliable  $^{14}\text{C}$  chronologies for loess deposits: Application to the loess sequence of nussloch (rhine valley, Germany). *Radiocarbon* 43, 611–618. doi:10.1017/s003822200041266
- Heiri, O., Lotter, A. F., and Lemcke, G. (2001). Loss on ignition as a method for estimating organic and carbonate content in sediments: Reproducibility and comparability of results. *J. Paleolimnol.* 25, 101–110. doi:10.1023/a:1008119611481
- Hu, M., Ji, T., Zheng, D., Zhuang, J., Sun, W., and Xu, A. (2022). The change characteristics of color parameters of eolian sediments and their environmental evolution in the northeastern qinghai-xizang plateau since 9.4ka. *Geoscience* 36, 439–448. doi:10.19657/j.geoscience.1000-8527.2022.014
- Ji, J., Shen, J., Balsam, W., Chen, J., Liu, L., and Liu, X. (2005). Asian monsoon oscillations in the northeastern Qinghai-Tibet Plateau since the late glacial as interpreted from visible reflectance of Qinghai Lake sediments. *Earth Planet. Sci. Lett.* 233, 61–70. doi:10.1016/j.epsl.2005.02.025
- Kalugin, I., Selegei, V., Goldberg, E., and Seret, G. (2005). Rhythmic fine-grained sediment deposition in Lake Teletskoye, Altai, Siberia, in relation to regional climate change. *Quat. Int.* 136, 5–13. doi:10.1016/j.quaint.2004.11.003
- Koinig, K. A., Shotyk, W., Lotter, A. F., Ohlendorf, C., and Sturm, M. (2003). 9000 years of geochemical evolution of lithogenic major and trace elements in the sediment of an alpine lake – The role of climate, vegetation, and land-use history. *J. Paleolimnol.* 30, 307–320. doi:10.1023/a:1026080712312
- Lamb, A. L., Wilson, G. P., and Leng, M. J. (2006). A review of coastal palaeoclimate and relative sea-level reconstructions using  $\delta^{13}\text{C}$  and C/N ratios in organic material. *Earth-Science Rev.* 75, 29–57. doi:10.1016/j.earscirev.2005.10.003
- Laskar, J., Fienga, A., Gastineau, M., and Manche, H. (2011). La2010: A new orbital solution for the long-term motion of the earth. *Astronomy Astrophysics* 532, A89. doi:10.1051/0004-6361/201116836
- Li, X., Liu, X., He, Y., Liu, W., Zhou, X., and Wang, Z. (2018). Summer moisture changes in the Lake Qinghai area on the northeastern Tibetan Plateau recorded from a meadow section over the past 8400 yrs. *Glob. Planet. Change* 161, 1–9. doi:10.1016/j.gloplacha.2017.11.016
- Liang, L., Sun, Y., Yao, Z., Liu, Y., and Wu, F. (2012). Evaluation of high-resolution elemental analyses of Chinese loess deposits measured by X-ray fluorescence core scanner. *Catena* 92, 75–82. doi:10.1016/j.catena.2011.11.010
- Lister, G. S., Kelts, K., Zao, C. K., Yu, J. Q., and Niessen, F. (1991). Lake Qinghai, China: Closed-basin like levels and the oxygen isotope record for ostracoda since the latest pleistocene. *Palaeogeogr. Palaeoclimatol. Palaeoecol.* 84, 141–162. doi:10.1016/0031-0182(91)90041-o
- Liu, X., Lai, Z., Yu, L., Sun, Y., and Madsen, D. (2012). Luminescence chronology of aeolian deposits from the Qinghai Lake area in the Northeastern Qinghai-Tibetan Plateau and its palaeoenvironmental implications. *Quat. Geochronol.* 10, 37–43. doi:10.1016/j.quageo.2012.01.016
- Liu, X., Colman, S. M., Brown, E. T., Henderson, A. C., Werne, J. P., and Holmes, J. A. (2014). Abrupt deglaciation on the northeastern Tibetan Plateau: Evidence from Lake Qinghai. *J. Paleolimnol.* 51, 223–240. doi:10.1007/s10933-013-9721-y
- Liu, Y., Liu, X., and Sun, Y. (2021). QGrain: An open-source and easy-to-use software for the comprehensive analysis of grain size distributions. *Sediment. Geol.* 423, 105980. doi:10.1016/j.sedgeo.2021.105980
- Liu, B. (2013). "Millennial-scale climate change in Holocene revealed by trace elements from eolian sediments in northeastern Tibetan Plateau," in *Journal of palaeogeography (Chinese edition)*. Editors Z. S. Heling Jin, Z. Su, and C. Zhang.
- Liu, X. (2018). Impact of temperature and precipitation changes in winter and summer on Holocene environmental change in Qinghai Lake, China. *J. Salt Lake Res.* 26, 11.
- Lu, H., Zhao, C., Mason, J., Yi, S., Zhao, H., Zhou, Y., et al. (2010). Holocene climatic changes revealed by aeolian deposits from the Qinghai Lake area (northeastern Qinghai-Tibetan Plateau) and possible forcing mechanisms. *Holocene* 21, 297–304. doi:10.1177/0959683610378884
- Lu, R., Jia, F., Gao, S., Shang, Y., Li, J., and Zhao, C. (2015). Holocene aeolian activity and climatic change in Qinghai Lake basin, northeastern Qinghai-Tibetan Plateau. *Palaeogeogr. Palaeoclimatol. Palaeoecol.* 430, 1–10. doi:10.1016/j.palaeo.2015.03.044
- Lv, Z. (2018). "Changes of aeolian sand activities since Holocene recorded in the East sandy land of Lake Qinghai lake, China," in *Arid land geography*. Editors X. L. Ruijie Lu, J. Du, L. Chen, and T. Li.
- Ma, Y., Zhang, J., Liu, X., and Lai, Z. (2011). Lake changes since Qinghai Lake's last deglaciation. *J. Salt Lake Res.* 19, 7.
- Meyers, P. A. (1990). Impacts of late Quaternary fluctuations in water level on the accumulation of sedimentary organic matter in Walker Lake, Nevada. *Palaeogeogr. Palaeoclimatol. Palaeoecol.* 78, 229–240. doi:10.1016/0031-0182(90)90216-t
- Meyers, P. A. (1994). Preservation of elemental and isotopic source identification of sedimentary organic matter. *Chem. Geol.* 114, 289–302. doi:10.1016/0009-2541(94)90059-0
- Ran, M., and Chen, L. (2019). The 4.2 ka BP climatic event and its cultural responses. *Quat. Int.* 521, 158–167. doi:10.1016/j.quaint.2019.05.030
- Richter, T. O., Van Der Gaast, S., Koster, B., Vaars, A., Gieles, R., De Stigter, H. C., et al. (2004). The Avaeatech XRF core scanner: Technical description and applications to NE atlantic sediments. *Geol. Soc. Lond. Spec. Publ.* 267, 39–50. doi:10.1144/gsl.sp.2006.267.01.03
- Santisteban, J. I., Mediavilla, R., Lopez-Pamo, E., Dabrio, C. J., Zapata, M., Garcia, M., et al. (2004). Loss on ignition: A qualitative or quantitative method for organic matter and carbonate mineral content in sediments? *J. Paleolimnol.* 32, 287–299. doi:10.1023/b:jopl.0000042999.30131.5b
- Shang, Y., Lu, R., Jia, F., Tian, L., Tang, Q., Chen, Y., et al. (2013). Paleoclimatic evolution indicated by major geochemical elements from aeolian sediments on the east of Qinghai Lake. *Sci. Cold Arid Regions* 5, 301–308. doi:10.3724/SP.J.1226.2013.00301
- Shen, J., Liu, X. Q., Wang, S. M., and Matsumoto, R. (2005). Palaeoclimatic changes in the Qinghai Lake area during the last 18,000 years. *Quat. Int.* 136, 131–140. doi:10.1016/j.quaint.2004.11.014
- Sun, Y., Lu, H., and An, Z. (2006). Grain size of loess, palaeosol and Red Clay deposits on the Chinese Loess Plateau: Significance for understanding pedogenic alteration and palaeomonsoon evolution. *Palaeogeogr. Palaeoclimatol. Palaeoecol.* 241, 129–138. doi:10.1016/j.palaeo.2006.06.018
- Sun, Y., Liang, L., Bloemendal, J., Li, Y., Wu, F., Yao, Z., et al. (2016). High-resolution scanning XRF investigation of Chinese loess and its implications for millennial-scale monsoon variability. *J. Quat. Sci.* 31, 191–202. doi:10.1002/jqs.2856
- Talbot, M. R., and Johannessen, T. (1992). A high resolution palaeoclimatic record for the last 27,500 years in tropical West Africa from the carbon and nitrogen isotopic composition of lacustrine organic matter. *Earth Planet. Sci. Lett.* 110, 23–37. doi:10.1016/0012-821x(92)90036-u
- Thomas, E. K., Huang, Y., Morrill, C., Zhao, J., Wegener, P., Clemens, S. C., et al. (2014). Abundant C4 plants on the Tibetan plateau during the lateglacial and early Holocene. *Quat. Sci. Rev.* 87, 24–33. doi:10.1016/j.quascirev.2013.12.014
- Utida, G., Cruz, F. W., Santos, R. V., Sawakuchi, A. O., Wang, H., Pessenda, L. C., et al. (2020). Climate changes in Northeastern Brazil from deglacial to Meghalayan periods and related environmental impacts. *Quat. Sci. Rev.* 250, 106655. doi:10.1016/j.quascirev.2020.106655

- Walker, M., Gibbard, P., Head, M. J., Berkelhammer, M., Björck, S., Cheng, H., et al. (2019). Formal subdivision of the Holocene series/epoch: A summary. *J. Geol. Soc. India* 93, 135–141. doi:10.1007/s12594-019-1141-9
- Wang, Y., Cheng, H., Edwards, R. L., He, Y., Kong, X., An, Z., et al. (2005). The Holocene Asian monsoon: Links to solar changes and North Atlantic climate. *Science* 308, 854–857. doi:10.1126/science.1106296
- Wang, Z., He, J., and Chen, Y. (2014). The reservoir effect of radiocarbon dating in lake sediment system. *J. DESERT Res.* 34, 683–688. doi:10.7522/j.issn.1000-694X.2014.000
- Wang, Z., Liu, Z., Zhang, F., Fu, M., and An, Z. (2015). A new approach for reconstructing Holocene temperatures from a multi-species long chain alkenone record from Lake Qinghai on the northeastern Tibetan Plateau. *Org. Geochem.* 88, 50–58. doi:10.1016/j.orggeochem.2015.08.006
- Weiss, H. (2019). “The 4.2 Ka BP Event in the Northern North Atlantic.” *Climate of the Past*. doi:10.5194/cp-2018-162-RC2
- Weiss, H. (2022). The East Asian summer monsoon, the Indian summer monsoon, and the midlatitude westerlies at 4.2 ka BP. *Proc. Natl. Acad. Sci.* 119, e2200796119. doi:10.1073/pnas.2200796119
- Yang, L., Sun, Y., E, C., Zhao, Y., and Lu, S. (2016). Geochemical element characteristics and paleoenvironmental significance of No. 1 Eolian section in Jiangxi Gully. *J. Salt Lake Res.* 24, 10.
- Yang, L., Long, H., Cheng, H., He, Z., and Hu, G. (2019). OS� dating of a mega-dune in the eastern Lake Qinghai basin (northeastern Tibetan Plateau) and its implications for Holocene aeolian activities. *Quat. Geochronol.* 49, 165–171. doi:10.1016/j.quageo.2018.02.005
- Yang, B., Qin, C., Bräuning, A., Osborn, T. J., Trouet, V., Ljungqvist, F. C., et al. (2021). Long-term decrease in Asian monsoon rainfall and abrupt climate change events over the past 6,700 years. *Proc. Natl. Acad. Sci.* 118, e2102007118. doi:10.1073/pnas.2102007118
- Yang, B., Qin, C., Bräuning, A., Osborn, T. J., Trouet, V., Ljungqvist, F. C., et al. (2022). Reply to Weiss: Tree-ring stable oxygen isotopes suggest an increase in Asian monsoon rainfall at 4.2 ka BP. *Proc. Natl. Acad. Sci.* 119, e2204067119. doi:10.1073/pnas.2204067119
- Zanchetta, G., Regattieri, E., Isola, I., Drysdale, R. N., Baneschi, I., and Hellstrom, J. C. (2016). The so-called “4.2 event” in the central Mediterranean and its climatic teleconnections. *Alp. Mediterr. Quat.* 29, 5–17.
- Zhang, J. (1998). “Response of numerical fluctuation of loss on ignition to past climate and environment characteristics in Beijing area,” in *Acta ecologica sinica*. Editor N. D. Zhaochen Kong.
- Zhou, W., Chui, Y., Yang, L., Cheng, P., Chen, N., Ming, G., et al. (2022). 14C geochronology and radiocarbon reservoir effect of reviewed lakes study in China. *Radiocarbon* 64, 833–844. doi:10.1017/rdc.2021.92